Search for Quark-Electron Compositeness in e^+e^- Production

The DØ Collaboration
URL http://www-d0.fnal.gov
(Dated: October 18, 2004)

We report preliminary results of a search for substructure in quarks and leptons assuming a four-fermion contact interaction for dielectron pairs of large invariant mass. The search is based on dielectron data collected by the DØ detector in $p\overline{p}$ collisions at $\sqrt{s}$=1.96 TeV. The results agree well with predictions of the standard model and we obtain model-dependent lower limits at 95% confidence level on the compositeness scale of 3.6 to 9.1 TeV for different chiral models of the composite structure of quarks and electrons.

Preliminary Results for Summer 2004 Conferences

I. INTRODUCTION

The proliferation of quarks and leptons has inspired speculations that they might be composite objects and bound states of more fundamental constituents. Models based on composite fermions and their constituents have been suggested that involve theories of nearly exact chiral symmetry based on the near-masslessness of fermions at higher energy scales [1]. Composite models have also been examined in the context of mass hierarchy of fermions and the number of generations. Below the characteristic energy scale that is called the compositeness scale Λ, the constituents ("preons") form composite bound states such as quarks and leptons. This binding interaction (sometimes termed metacolor) can be modeled as a four-fermion contact interaction represented by a Lagrangian ($\mathcal{L}$) well below energies corresponding to Λ [2]

$$\mathcal{L} = \frac{4\pi}{\Lambda^2}[\eta_{LL}(\overline{q_L}\gamma^\mu q_L)(\overline{e_L}\gamma_\mu e_L) + \eta_{LR}(\overline{q_L}\gamma^\mu q_L)(\overline{e_R}\gamma_\mu e_R) + \eta_{RL}(\overline{q_R}\gamma^\mu q_R)(\overline{e_L}\gamma_\mu e_L) + \eta_{RR}(\overline{q_R}\gamma^\mu q_R)(\overline{e_R}\gamma_\mu e_R)] \quad (1)$$

where q=(u,d) represents the first-generation quarks, e represents (e,ν), η is a sign factor that is - for constructive and + for destructive interference, L(R) denotes left (right) helicity of quark or lepton currents. The presence of such contact interaction would produce significant deviations in the e^+e^- production relative to theory at large invariant mass [3]. Thus a precision measurement of the Drell-Yan cross section can provide signature for this kind of interaction and the presence of new physics at the TeV scale. In the absence of a deviation from the standard model (SM), the observed e^+e^- cross section can be used to set a lower limit for the scale of compositeness.

In Run I, DØ reported a limit on compositeness of 3.3 TeV to 6.1 TeV that depended on the type of chiral model used in the analysis [4]. In Run I, in addition to the dilepton and $W \rightarrow e\nu$ channels, DØ and CDF also studied compositeness using dijet mass and angular distributions. These yielded poorer limits on possible compositeness scales [5, 6]. The SM cross section for high-mass lepton pair production is smaller than the $q\bar{q}$ scattering cross section by a factor of order $(\alpha_{em}/\alpha_s)^2$. Nevertheless, dilepton channels are more sensitive than hadron final states. In fact, the most stringent limits on Λ are from atomic parity violation experiments, and some phenomenological analysis has even suggested a possible contact interaction scale $\sim$11 TeV to accomodate certain anomalous results [7]. A direct search for a contact interaction by the HERA H1 collaboration yields limits on compositeness scale that range between 1.3 to 5.5 TeV [8]. Besides considering parity-violating composite-fermion models, we have extended our analysis to include the parity-conserving and other symmetric terms in $\mathcal{L}$, which could not be studied in atomic experiments [9].

II. DIFFERENT MODELS OF COMPOSITENESS

The observable consequences of quark and lepton compositeness are highly model-dependent and can be classified according to the corresponding left or right helicity projections in the Lagrangian. However, we can also write the total dilepton cross section σ_T modified by a contact interaction, in the general form

$$\frac{d\sigma_T}{dM} = \frac{d\sigma_{sm}}{dM} + \frac{I}{\Lambda^2} + \frac{C}{\Lambda^4} \quad (2)$$

where M is the dilepton invariant mass, σ_{SM} is the contribution from the SM, I is the interference of SM with the contact term and C is the contact term alone (see Fig. 1). The cross section is defined by the compositeness scale and sign of the interference (I and C are not independent). To avoid more assumptions regarding intergeneration symmetry we consider only the dominant light-quark contribution in the contact term.

We use the ratio of leading-order LO (with LO parton distributions-PDF) and next-to-LO (NLO) (with NLO PDF) calculated cross sections to define a correction K factor 1.37 to our program, and assume the same correction for compositeness. We assign a systematic uncertainty of 10% on K.

III. DATA ANALYSIS

A. Detector

This analysis is based on $\overline{p}p$ data collected by DØ detector from Sept. 2002 to March 2004 during Tevatron Run II $p\overline{p}$ collisions at $\sqrt{s}$=1.96 TeV. The total integrated luminosity for this dataset is 271±17 pb^{-1}.

The DØ detector is comprised of central-tracking system located within a 2 T superconducting solenoidal magnet, a liquid-argon uranium calorimeter and a muon spectrometer [11]. The central-tracking system, which consists
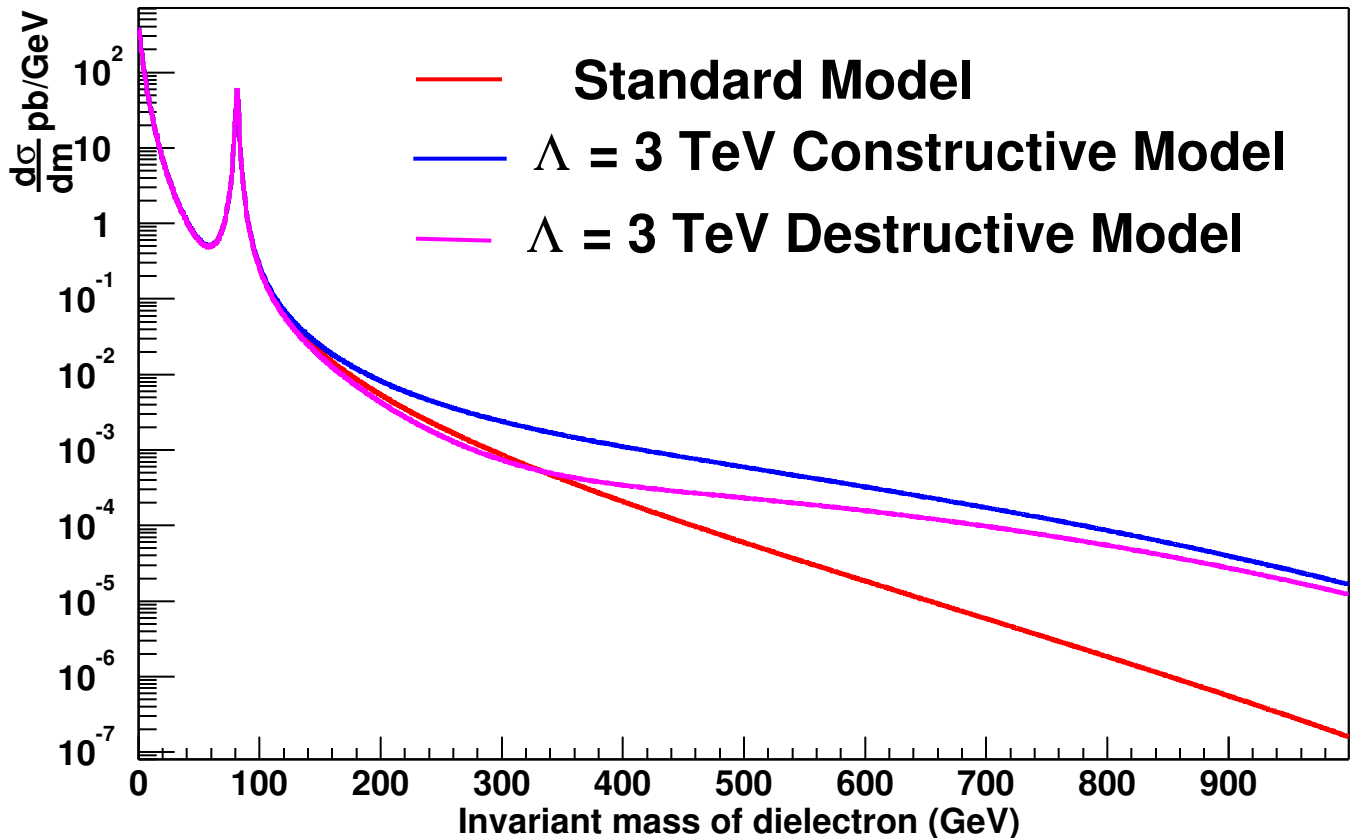
FIG. 1: Differential cross section for e^+e^- production for constructive and destructive interference of compositeness term with standard model as a function of e^+e^- mass

of a silicon microstrip tracker (SMT) and a central fiber tracker (CFT) has tracking and vertexing capability at pseudorapidities of $|\eta| < 3$. Central and forward preshower detectors located just outside of the superconducting coil (in front of the calorimetry) are constructed of several layers of extruded triangular scintillator strips that are read out using wavelength-shifting fibers and VLPCs. The next layer of detection involves three liquid-argon/uranium calorimeters: a central section (CC) covering $|\eta|$ up to ≈ 1, and two end calorimeters (EC) extending coverage to $|\eta| \approx 4$, all housed in separate cryostats [10]. In addition to the preshower detectors, scintillators between the CC and EC cryostats provide sampling of developing showers at $1.1 < |\eta| < 1.4$. A muon system resides beyond the calorimetry, and consists of a layer of tracking detectors and scintillation trigger counters before 1.8 T toroids, followed by two more similar layers after the toroids. Tracking at $|\eta| < 1$ relies on 10 cm wide drift tubes [10], while 1 cm mini-drift tubes are used at $1 < |\eta| < 2$. Luminosity is measured using plastic scintillator arrays located in front of the EC cryostats, covering $2.7 < |\eta| < 4.4$.

B. Event Selection

Events must pass a set of high p_T electron triggers designed to accept electrons with large transverse momenta (p_T). Events are required to have two electromagnetic (EM) objects in the calorimeter with $p_T > 25$ GeV/c. Both EM objects must be in the fiducial region of the detector. In central region of calorimeter (CC), electrons must have $|\eta_{det}| < 1.1$ and in the forward regions or end calorimeters (EC), we select electrons with $1.5 \leq |\eta_{det}| < 2.4$. The pseudorapidity η_{det} is defined relative to the center of the detector. We define "loose" electrons by the fraction of EM energy deposited in the EM layer of a calorimeter,by degree of isolation, and the shape of the electron shower in calorimeter. The more reliable "tight" electrons, in addition, require a matching track extrapolated from the central tracker. In the final data sample, we require at least one tight electron.

C. Calculation of Efficiency

Total detection efficiency can be factorized in terms of a trigger efficiency, an electron identification efficiency and a track-matching efficiency multiplied by the acceptance efficiency of the detector. Since other efficiencies are essentially independant of invariant mass, only the acceptance efficiency is calculated using Monte Carlo samples of $Z \to ee$ decays that are passed through the DØ Geant simulation chain generated for different e^+e^- mass bins [12]. The MC sample is in good agreement with the $Z \to ee$ data. Efficiencies are calculated separately for events with both electrons in the CC and for those with one electron in the CC and one in the EC,and found to be practically insensitive to the compositeness scale.

Uncertainties on efficiency are dominated by systematics (4% in total), which accounts for different uncertainty in PDF, EM scale, resolution and radiation. In addition, we have a 5% systematic uncertainty for any dependence on η. The uncertainties from all sources are added in quadrature. Only the statistical uncertainties are given in Table I.

Mass (GeV)	Efficiency
120-160	0.56±0.01
160-200	0.58±0.01
200-240	0.59±0.01
240-290	0.59±0.01
290-340	0.60±0.01
340-400	0.60±0.01
400-500	0.61±0.01
500-600	0.62±0.01
600-1000	0.62±0.01

Table I. Total acceptance and its statistical uncertainty as a function of e^+e^- mass.

IV. BACKGROUND STUDIES

A. Rate for Jets Mimicing Electrons

The background is due mainly to jets misidentified as electrons, two chief sources being multijet(dijet) and γ+jet events, where both jets, or a photon and a jet,respectively, pass electron identification. To study this, we select single-EM triggers requiring one EM object with $p_T > 25$ GeV/c and $\not{E}_T < 15$ GeV to remove $W \to e\nu$ events. These criteria assume removal of most true single electrons produced by the SM physics processes. The majority of these events are from multijet production where one jet is reconstructed as an EM object. Thus, we can obtain the rate for jets to mimic electrons as a function of p_T for tight and loose EM objects. The $\gamma +$ jet channel also contributes to e^+e^- background. We take this into account through a weighted probability in the total jet spectrum, as discussed in the next section.

B. Background γ +jets and Multijets

The background from multijets is determined from the same diEM sample as used for signal for two EM objects. We require each EM object to have $p_T > 25 GeV/c$ and appropriate η. But now we reverse the shower-shape cut requirements for electrons, and require poor electron identification. This sample is then dominated by multijet events (photon contamination is negligible). Now, we obtain the background by multiplying the previous rate to mimic electrons by the probability of each event as reflecting contribution from the dijet (or multijet) and photon-jet, where photon-jet contribution is estimated by the ratio of dijet and photon-jet production cross-sections (table II).

E_T range (GeV)	$\frac{\sigma_{dijet}}{\sigma_{\gamma jet}}$
20-40	2576
40-80	1516
80-160	807
160-320	359
320-980	155

Table II. Ratio of dijet and photon-jet production cross-sections with E_T
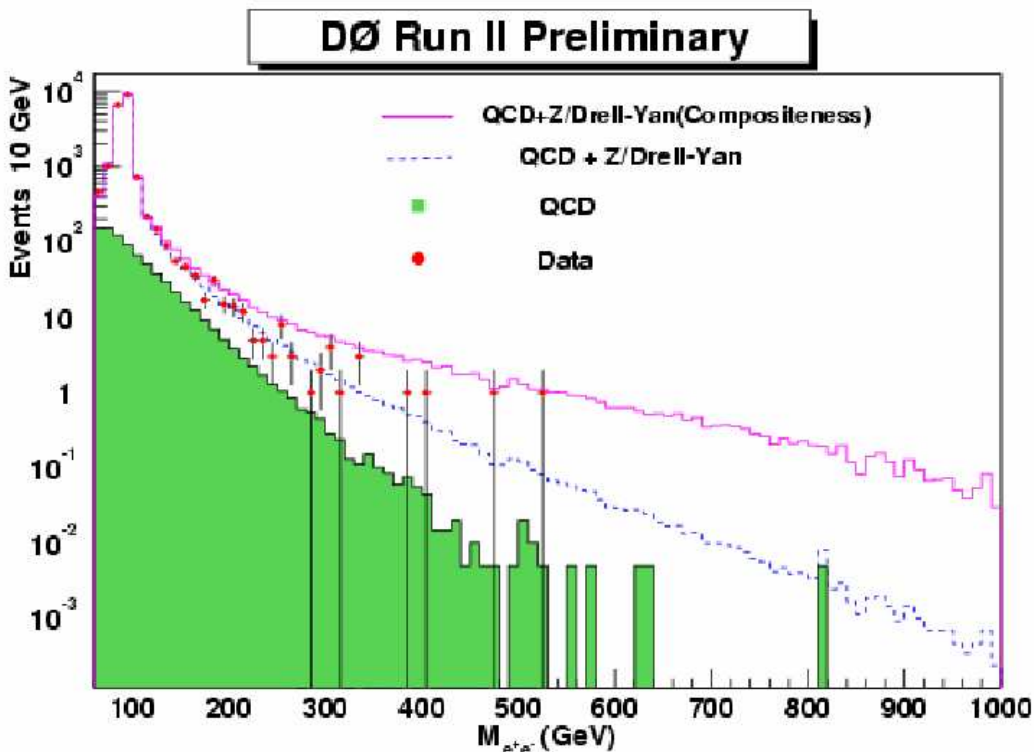
FIG. 2: Dielectron invariant mass distributions for QCD background (solid histogram), the standard model and a model with $\Lambda = 3$ TeV and left-handed quark and lepton helicities (open histograms), and the data (points with error bars.)

C.   Other Small Backgrounds

Other backgrounds to e^+e^- production are small compared to all-jet and $\gamma + jet$ ("QCD") background. These have been added in the final calculation, using a fast detector simulation, where generated events are properly weighted with cross sections. These contribute at $< 1\%$ of the level of standard QCD processes (e.g. $t\bar{t} \to$ ee, $W\gamma \to$e$\nu\gamma$, $Z\gamma \to$ eeγ , $WW \to$ ee, $\gamma^*/Z \to \tau\tau \to$ee).

D.   Expected Background

As we have indicated, the main background to the SM Drell-Yan $Z/\gamma*$ process background is from standard jets, termed QCD below. Other processes do not contribute significantly. The invariant mass spectrum in the MC is smeared by 4.2% to match with the data. The number of events in the Z region be expressed as:

$$N_{data} = f_{Z/\gamma*} * N_{Z/\gamma*} + f_{QCD} * N_{QCD} \tag{3}$$

where $f_{Z/\gamma*}$ and f_{QCD} are best-fit normalization constants, whose values are determined through a fit of signal ($N_{Z/\gamma*}$) and background (N_{QCD}) to data in the 60-130 GeV region. This provides the total number of background events because $N_{Z/\gamma*}$ and N_{QCD} are known from Monte Carlo and data respectively. For the higher mass region, we use only number of QCD events to represent background (ignoring the smaller sources such as $t\bar{t}$ etc). Fit in the Z region gives 4%(6%) uncertainty for CC(EC) results. The difference between calculated background following the same method but for 65-115 GeV region, is taken as the systematic uncertainty on normalization, which is about 7% (8.5%).

V.   COMPARISON OF DATA WITH STANDARD MODEL

Table III shows the observed and expected number of events, normalized to the data in the Z region (See fig. 2).

Mass (GeV)	Observed events	Expected (QCD)	Expected (QCD+DY)
120-160	343	154.25±24.1	350.38±28.5
160-200	99	43.3±8.43	107±9.4
200-240	36	14.0±2.7	40.8±3.3
240-290	15	5.67±1.1	20.1±1.5
290-340	10	1.7±0.3	8.3±0.8
340-400	1	0.76±0.15	4.3±0.31
400-500	2	0.101±0.02	2.2±0.17
500-600	1	0.04±0.01	0.69±0.05
600-1000	0	0.02±0.01	0.31±0.02

Table III. Observed and expected number of events.

VI.   LIMITS ON SCALE OF COMPOSITENESS

We have obtained a mass distribution for dielectron data that agrees well with predictions of the standard model. Using a Bayesian approach, as in Run I [4], we obtain a stronger limit for the compositeness scale. Our method requires priors of efficiency (ϵ), luminosity ($\mathbf{L}$) and background (b) in addition to the cross section at each invariant mass for different compositeness scales. We define a likelihood function, using a flat prior for cross section, and Gaussian priors for efficiency, luminosity and background. The joint probability for all mass bins is a function of Λ and the distribution is normalized to unit probabilty [4].

$$P(\frac{1}{\Lambda^2}) = \frac{1}{N} \int_0^\infty db \int_0^\infty d\mathbf{L} \prod_{k=1}^n \int_0^1 d\epsilon \frac{\exp^{-N_{pred}} N_{pred}^{N_{obs}}}{N_{obs}!} P(b).P(\mathbf{L}).P(\epsilon).P(\sigma^k) \tag{4}$$

N is the normalization constant, $P(\frac{1}{\Lambda^2})$ is the posterior probability density, $P(b), P(\mathbf{L})$ and $P(\epsilon)$ are the Gaussian priors for efficiency, luminosity and background,. $P(\sigma^k)$ is the flat prior for cross section in k-th bin. N_{pred} and N_{obs} are the number of expected and observed events. To get limits on Λ this distribution is integrated for 95% CL (Fig.3).

$$\int_{\Lambda_{limit}}^\infty P(\frac{1}{\Lambda^2}) d\sigma^{'} = 0.95 \tag{5}$$

Limits are set for each of the parity violating terms LL, RR, RL, LR in the contact interaction $\mathcal{L}$, where first letter denotes quark current and second letter denotes lepton current. We have also considered parity conserving terms or other symmetric combinations of these terms (table IV), such as LL+RR, LR+RL, LL-LR, RL-RL, vector-vector (VV= LL+RR+RL+LR) and axial vector -axial vector (AA = LL+RR-RL-LR) for setting limits separately (Fig 4).

Model	$\Lambda-$ (TeV)	$\Lambda+$ (TeV)
LL	6.2	3.6
RL	5.0	4.3
LR	4.8	4.5
RR	5.8	3.8
LL+RR	7.9	4.1
LR+RL	6.0	5.0
LL-LR	6.4	4.8
RL-RR	4.7	6.8
VV	9.1	4.9
AA	7.8	5.7

Table IV. Limits of compositeness scale Λ for different chiral models

VII.   CONCLUSIONS

We have studied the dielectron invariant mass spectrum at high mass for Run II DØ data. We find the observed number of events are in good agreement with the standard-model prediction for background. No evidence of new physics has been observed, and we therefore, extract limits on the compositeness scale Λ for quark-electron compositeness scale ranging from 3.6 to 9.1 TeV, which are improved considerably relative to the limits 3.3 to 6.1 TeV in Run I.
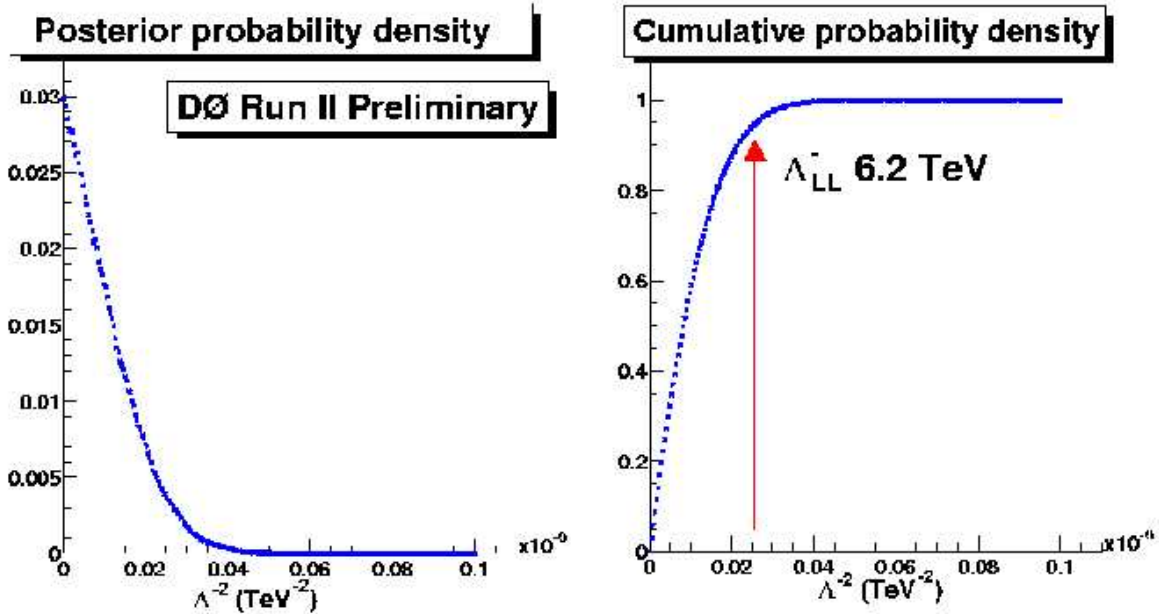
FIG. 3: Posterior (left) and Cumulative (right) probability distributions as a function Λ^{-2} in TeV^2 limits. The arrow shows the 95% CL limit. Λ^-_{LL} denotes the scale of compositeness for constructive interference.

[1] G.'t Hooft, in Recent Developments in Gauge Theories (Cargese Summer Institute, 1979), edited by G.'t Hooft et al. (Plenum, New York,1980),p135; S. Dimopolous, S. Raby and L. Susskind Nucl. Phys. **B173**, 208 (1980); J.L. Rosner, Workshop on New Strong Dynamics for Run-II of Fermilab Tevatron, hep-ph/9812537.
[2] E. Eichten,K. Lane and M. Peskin, Phys. Rev. Lett. **50**, 811 (1983); E. Eichten,I. Hinchliffe,K. Lane and C. Quigg, Rev. Mod. Phys. **56**, 579 (1984);
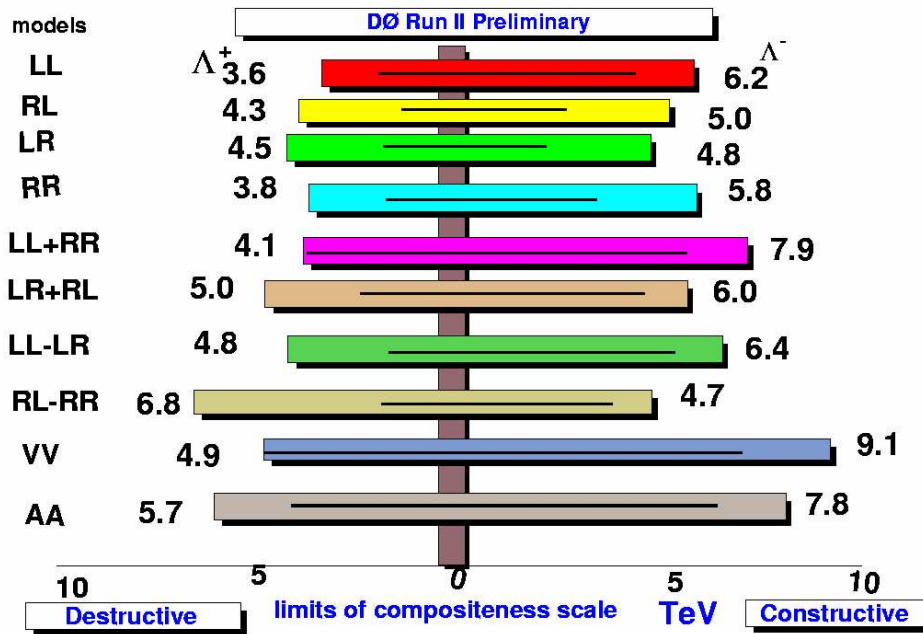
FIG. 4: Limits for scale of compositeness are shown for various chiral models with solid excluded region. Black lines show RunI limit

T Lee, Phys. Rev. D. **55**, 2591 (1997).

[3] S. D. Drell and T. M. Yan, Phys. Rev. Lett. **25**, 316 (1970).

[4] DØ Collaboration, B. Abbot *et al.*, Phys. Rev. Lett. **82**, 4769 (1999).

[5] DØ Collaboration, B. Abbot *et al.*, Phys. Rev. D Rapid Comm. **62**, 031101 (2000);
B. Abbot *et al.* Phys. Rev. Lett. **82**, 2457 (1999);
B. Abbot *et al.*, Phys. Rev. Letters **80**, 666 (1998).

[6] CDF Collaboration T. Affolder *et al.*, Phys. Rev. Lett. **87**, 231803 (2001);
F. Abe et al. Phys. Rev. Lett. **79**, 2198 (1997).

[7] V. Barger *et al.*, Phys. Lett. **B 480**, 149 (2000).

[8] H1 Collaboration C. Adloff *et al.*, Phys. Lett. **B 479**, 358 (2000).

[9] A. Nelson, Phys. Rev. Lett. **78**, 4159 (1997);
S. Bennet and C. Wieman, Phys. Rev. Lett. **82**, 2484 (1999).

[10] S. Abachi, *et al.*, Nucl. Instrum. Methods Phys. Res. **A 338**, 185 (1994).

[11] V. Abazov, et al., in preparation for submission to Nucl. Instrum. Methods Phys. Res. A;
T. LeCompte and H.T. Diehl, "The CDF and DØ Upgrades for Run II", Ann. Rev. Nucl. Part. Sci. **50**, 71 (2000).

[12] R. Brun and F. Carminati, CERN Program Library Long Writeup W5013, 1993 (unpublished).